Supporting Information for

Pt nanoparticles grown on 3D RuO_2-modified graphene architectures for highly efficient methanol oxidation

Huajie Huang,*[a] Jixin Zhu,[b] Debo Li,[a] Chao Shen,[a] Miaomiao Li,[a] Xin Zhang,[a] Quanguo Jiang,[a] Jianfeng Zhang,*[a] and Yuping Wu[a]

[a]*College of Mechanics and Materials, Hohai University, Nanjing 210098, China*

[b]*Key Laboratory of Flexible Electronics (KLOFE) & Institute of Advanced Materials (IAM), Jiangsu National Synergetic Innovation Center for Advanced Materials (SICAM), Nanjing Tech University (Nanjing Tech), 30 South Puzu Road, Nanjing 211816, China*

**Corresponding authors.*

E-mail address: huanghuajie@hhu.edu.cn (H. Huang), jfzhang@hhu.edu.cn (J. Zhang)

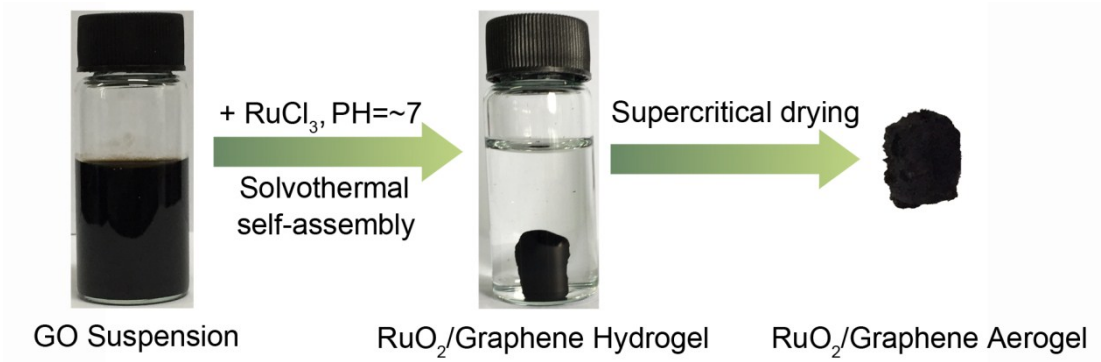

Fig. S1 The synthetic process for RuO_2/graphene hybrid aerogel. It includes: (1) mixture of GO suspension, $RuCl_3$ and NaOH by magnetic stirring and ultrasonic treatment; (2) fabrication of RuO_2/graphene hydrogel through a solvothermal reaction; (3) formation of RuO_2/graphene aerogel by supercritical drying.

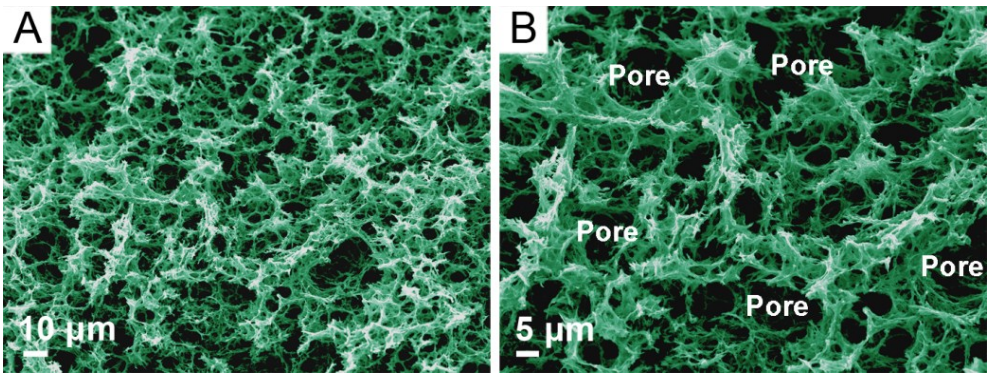

Fig. S2 FE-SEM images of the Pt/RuO_2/G architecture at different magnifications, showing that the sample possesses an interconnected 3D porous structure.

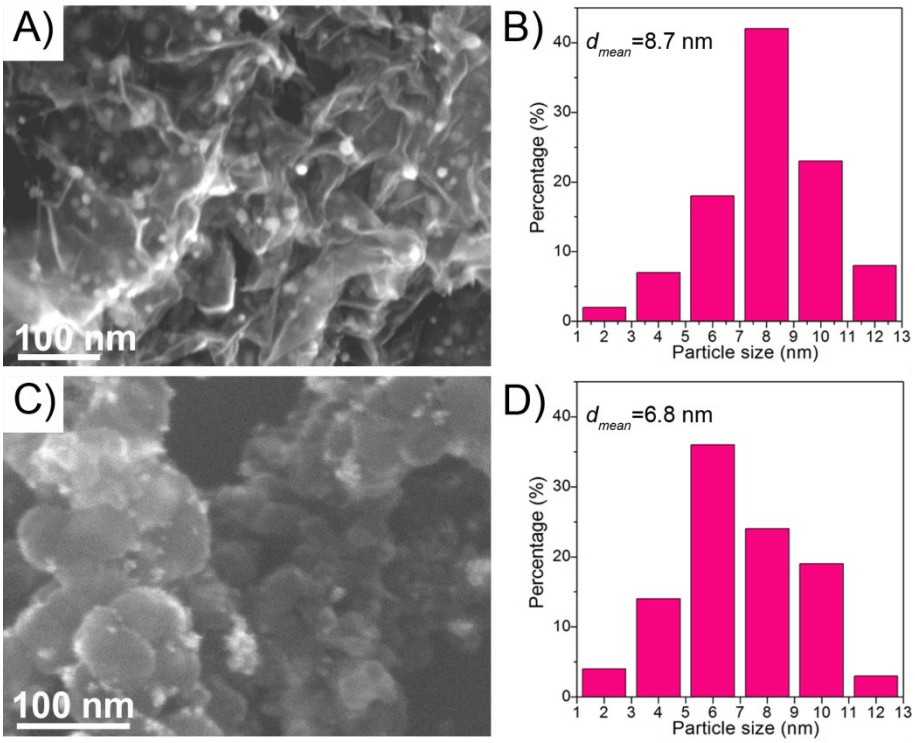

Fig. S3 Representative FE-SEM images and Pt particle size distribution of (A and B) Pt/G and (C and D) Pt/C, respectively. It can be seen that the Pt particles in these samples have much larger sizes when compared with that of Pt/RuO_2/G architecture.

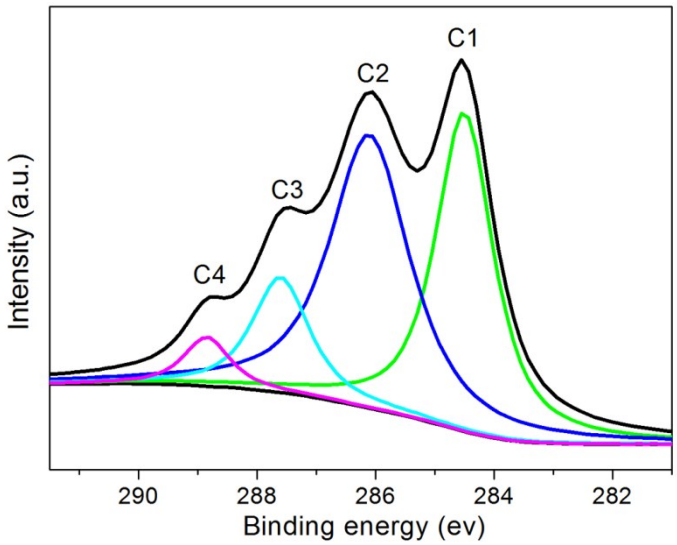

Fig. S4 C 1s core-level XPS spectrum of GO suggests that there are a large number of oxygen functional groups on GO sheets.

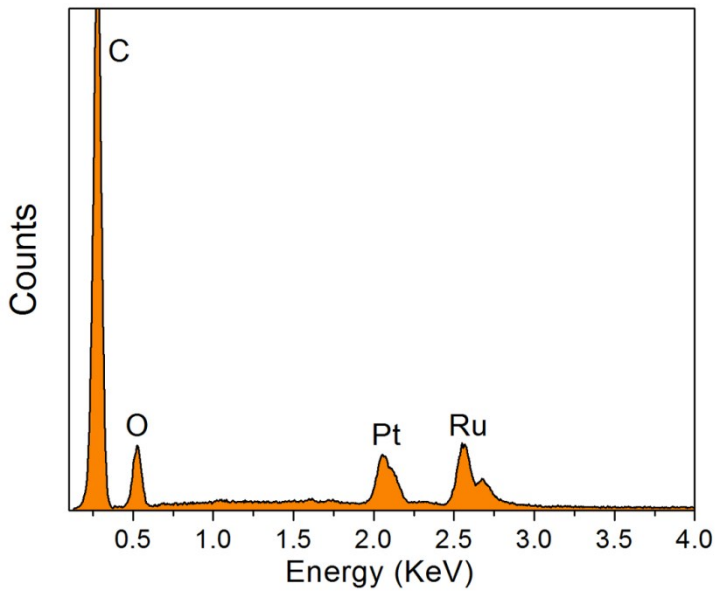

Fig. S5 EDX spectrum of the Pt/RuO_2/G architecture, showing that the sample mainly contains C, O, Pt and Ru elements.

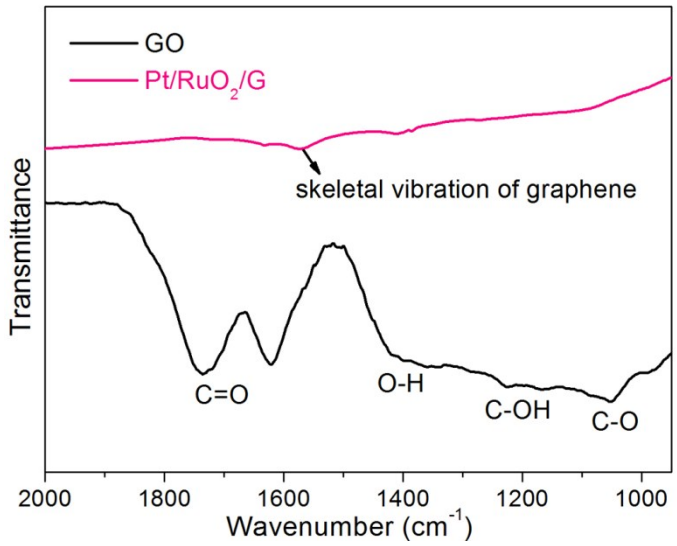

Fig. S6 FT-IR spectra of GO and Pt/RuO_2/G imply the successful reduction of GO to graphene during the solvothermal process.

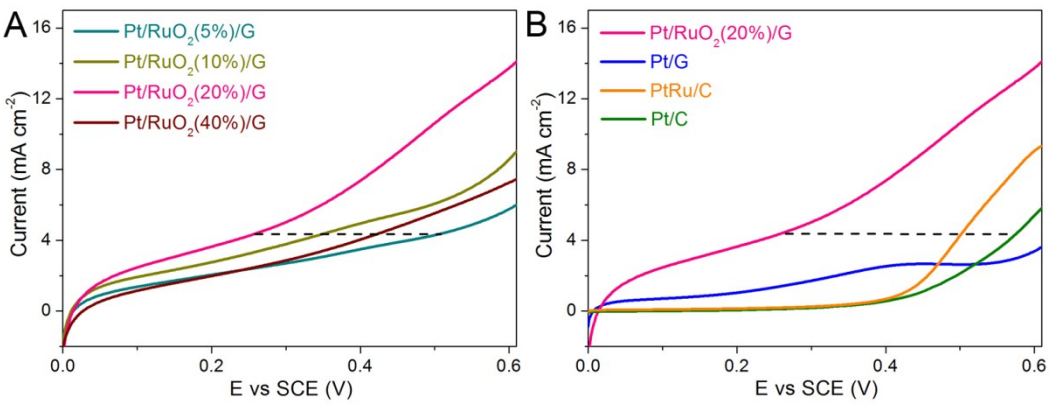

Fig. S7 Linear sweep voltammetrys of (A) the Pt/RuO_2/G architectures with varying RuO_2 contents, and (B) Pt/RuO_2(20%)/G, Pt/G, PtRu/C, and Pt/C in 1 M H_2SO_4 with 2 M methanol solution at a scan rate of 20 mV s^{-1}. At a given current density, the Pt/RuO_2(20%)/G architecture possesses an apparently lower potential than other catalysts, indicating that the catalytic reaction could occur much more easily with the help of Pt/RuO_2(20%)/G.

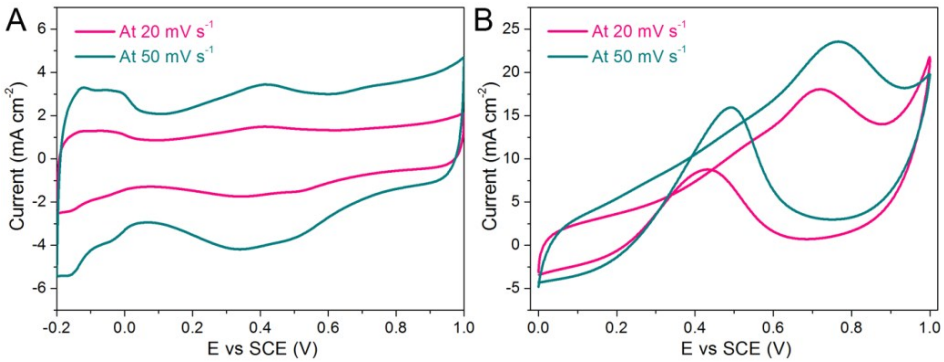

Fig. S8 (A) CV curves of the Pt/RuO_2(20%)/G catalyst in 1 M H_2SO_4 solution with different scan rates. (B) CV curves of the Pt/RuO_2(20%)/G catalyst in 1 M H_2SO_4 and 2 M methanol solution with different scan rates.

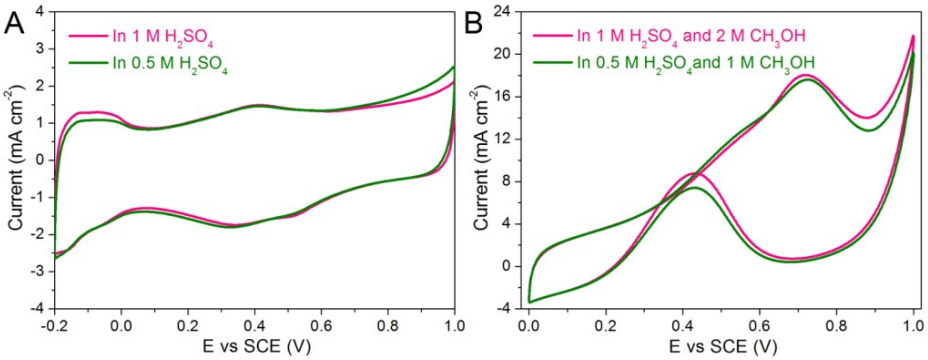

Fig. S9 (A) CV curves of the Pt/RuO_2(20%)/G catalyst in H_2SO_4 solutions with different concentrations at 20 mV s^{-1}. (B) CVs of the Pt/RuO_2(20%)/G catalyst in mixture of H_2SO_4 and methanol solutions with different concentrations at 20 mV s^{-1}.

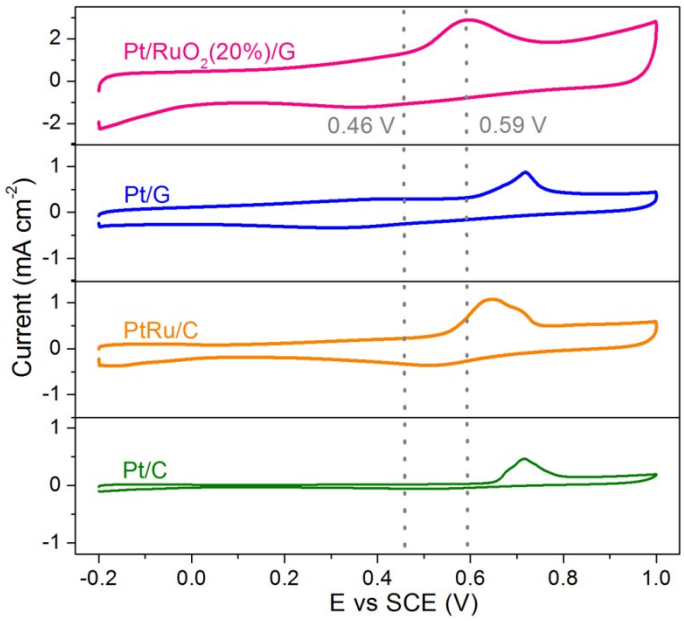

Fig. S10 CO stripping voltammograms for Pt/RuO_2(20%)/G, Pt/G, PtRu/C, and Pt/C catalysts recorded in 1 M H_2SO_4 solution at a scan rate of 20 mV s^{-1}, suggesting that Pt/RuO_2(20%)/G has the best anti-poisoning ability.

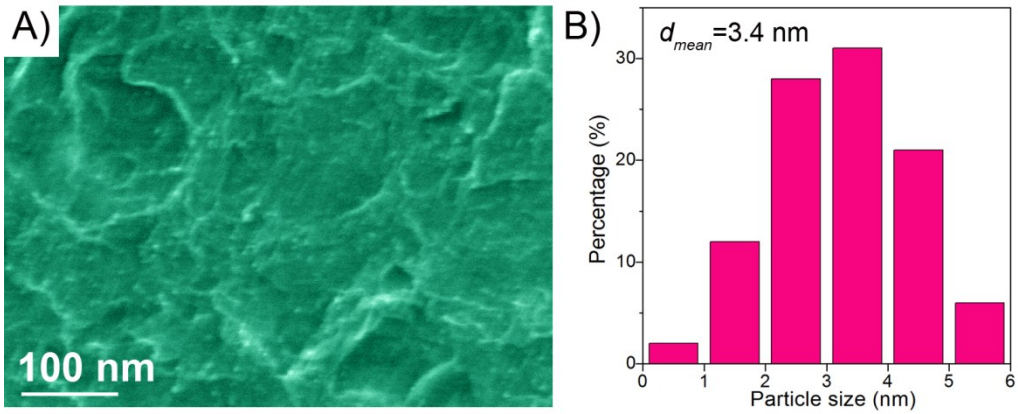

Fig. S11 Typical (A) FE-SEM image and (B) Pt particle size distribution of Pt/RuO_2(20%)/G architecture after the long-term chronoamperometric tests, revealing that the microstructure of Pt/RuO_2(20%)/G was well preserved under the electrocatalytic conditions.

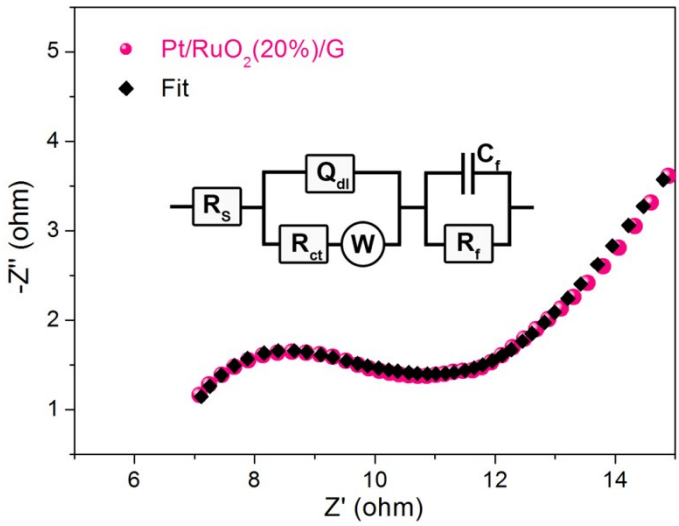

Fig. S12 Nyquist plots of Pt/RuO_2(20%)/G electrode and the corresponding fitting curve, showing a good match between the experimental and fitting results. The inset is the equivalent circuit: R_s and R_{ct} represent the resistances of electrolyte and electrocatalyst, respectively, Q_{dl} is a constant phase element, W corresponds to semiinfinite diffusion at the interface between electrolyte and hybrid catalyst, R_f and C_f represent the resistance and capacitance of the Nafion-carbon film, respectively.